Crystal Growth and Agglomeration of Calcium Sulfite Hemihydrate Crystals

Clifford Y. Tai, and Pao-Chi Chen

Ind. Eng. Chem. Res., **1995**, 34 (4), 1342-1351 • DOI: 10.1021/ie00043a040

Crystal Growth and Agglomeration of Calcium Sulfite Hemihydrate Crystals

Clifford Y. Tai*

Department of Chemical Engineering, National Taiwan University, Taipei, Taiwan 10617, ROC

Pao-Chi Chen

Department of Chemical Engineering, Long-Hau Junior College, Tao-Yuan, Taiwan, ROC

Crystal growth and agglomeration of calcium sulfite hemihydrate crystals from solution were studied by reacting $Ca(OH)_2$ with $NaHSO_3$ in a pH-stat semibatch crystallizer. Single platelet crystals and agglomerates of platelet crystals were produced in the pH range from 5.80 to 6.80. The crystallization mechanism changed from primary nucleation to crystal growth in the progressive precipitation. Using the titration curves, the growth rate was calculated from the titration rate at the final stage of operation. The crystal growth rates of calcium sulfite hemihydrate crystals were found to obey the parabolic rate law in the low supersaturation range. Another point to be noted is that the precipitates of calcium sulfite hemihydrate in agitated suspensions have a tendency to form agglomerates. It was found that the degree of agglomeration is a weak function of relative supersaturation and magma density, while the pH value is a key factor that affects the degree of agglomeration. Addition of EDTA also has an effect on the agglomeration of calcium sulfite hemihydrates.

Introduction

Flue gas desulfurization (FGD) processes are most commonly utilized to remove sulfur dioxide from stack gases of coal- or oil-fired plants. Many FGD processes, including throwaway processes, gypsum processes, and regenerative processes, have been developed over the last 30 years, and several processes are being used successfully in full scale. In the simple slurry technology, SO_2 is absorbed by a slurry of lime/limestone to form calcium sulfite crystals of acicular habit and its strong agglomeration, requiring large clarifiers and filters to dewater the sludge to make an acceptable landfill. On the other hand, the double alkali processes are being investigated to overcome the scaling, plugging, erosion, and dewatering problems that have been associated with the lime/limestone systems. Besides, high SO_2 removal efficiencies and high lime/limestone utilizations are easily achieved with alkaline sodium scrubbing solutions by simply adjusting the scrubber operating pH (Valencia, 1982).

In the lime dual-alkali process, the absorption of SO_2 with chemical reaction in the scrubber is

$$Na_2SO_3 + SO_2 + H_2O \rightarrow 2NaHSO_3$$

Then, the scrubber solution is pumped into a crystallizer and reacts with $Ca(OH)_2$ solution transported from a storage tank. The major reaction equation in the crystallizer is

$$2NaHSO_3 + Ca(OH)_2 \rightarrow CaSO_3{\cdot}{}^1/_2H_2O(s) + {}^3/_2H_2O + Na_2SO_3$$

The clear solution, Na_2SO_3 solution in the crystallizer, is repumped into the scrubber for reusing. The calcium salt of $CaSO_3{\cdot}{}^1/_2H_2O(s)$ was obtained with good settling and filtration characteristics in a pilot scale operation (LaMantia et al., 1975; Satriana, 1981).

Crystal morphology and size affect the dewatering process, including sedimentation and filtration, and they are key factors leading to a successful operation of a FGD process (Tseng and Rochelle, 1986; Dirksen and Ring, 1991). Crystal morphology could be modified by solution composition, additives, and solution pH, which also influence the crystal growth rate (Dirksen and Ring, 1991; Chen et al., 1992). The dewatering process proceeded more easily for crystals in platelet form as compared with crystals in acicular form (Ottmers, 1974; Phillips, 1978).

Agglomeration complicates the analysis of crystal size distribution (CSD) when using the batch and MSMPR crystallizer data. Several methods were proposed to investigate the effect of agglomeration on the CSD, such as agglomeration kernel functions (Beckman and Farmer, 1987; Hostomsky and Jones, 1991; Tavare and Garside, 1993) and the degree of agglomeration (Budz et al., 1986; Söhnel and Mullin, 1992; Tai and Chen, 1994). In those studies, they found that the degree of agglomeration was a function of relative supersaturation, stirring speed, and solid concentration. In order to characterize the changes in CSD, the parameters, such as the total number of crystals, N_t, the number of large crystals greater than some arbitrary size, L_0, and the mass-weighted average size, $L_{4,3}$, are utilized to quantify the degree of agglomeration (Hartel et al., 1986). When the agglomeration occurs, a decrease in the total number of particles, an increase in the number of large particles, and hence an increase in the mass-weighted average size would be observed.

To study the crystal growth of sparingly soluble salts, such as calcium sulfide hemihydrate and calcium carbonate, unseeded experiments (Klepetsanis and Koutsoukos, 1989; Kralj et al., 1990) and seeded experiments (Christoffersen and Christoffersen, 1990; Tai et al., 1993) have been applied. In these experiments, the pH-stat apparatus is most commonly employed (Tseng and Rochelle, 1986; Christoffersen and Christoffersen, 1990; Tai et al., 1993). From the titration curve (Klepetsanis

0888-5885/95/2634-1342$09.00/0

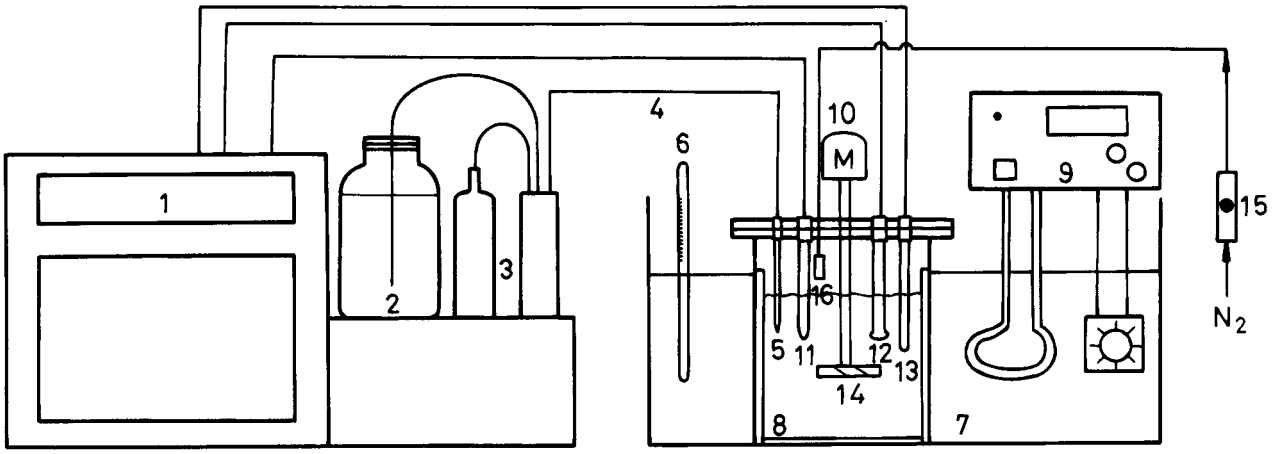

Figure 1. pH-stat semibatch crystallization system: 1, pH and temperature indicator; 2, reagent bottle; 3, pumping system of reagent; 4, reagent deliver line; 5, burette; 6, thermometer; 7, water bath; 8, crystallizer; 9, temperature controller; 10, motor; 11, glass electrode; 12, reference electrode; 13, thermocompensator; 14, axial-flow impeller; 15, rotameter; 16, sparging tube.

and Koutsoukos, 1989; Tai et al., 1993) and the concentration–time curve (Kazmlerczak et al., 1982), the growth rates can be calculated.

The aim of this work was to search for the operating conditions that would form the platelet crystals of calcium sulfite hemihydrate and to determine the growth mechanism of platelet $CaSO_3{\cdot}^1/_2H_2O$ using a pH-stat apparatus. The $Ca(OH)_2/NaHSO_3/H_2O$ reacting system was performed without seeding. The crystallization process began with an increase of primary nuclei followed by crystal growth. The growth rate of calcium sulfite hemihydrate was calculated from the titration curves using the method proposed in this work. In addition, the degree of agglomeration of calcium sulfite hemihydrate crystals was assessed and correlated with operating variables in order to have a better understanding of the agglomeration mechanism.

Experimental Apparatus and Procedure

The crystallization system of the semibatch study of calcium sulfite hemihydrate is shown in Figure 1. The acrylic plastic crystallizer was placed in a thermostated water bath at 25 °C. The diameter and height of the crystallizer are 120 and 140 mm, respectively. The crystallizer is baffled with four longitudinal baffles, of which the thickness is 10 mm each, at 90° spacing. The diameter of the stirrer, an axial-flow glass-made agitator, is 50 mm. The stirring rate was set at 400 rpm to suspend the crystals. One liter of supersaturated solution of calcium sulfite was prepared by adding calcium hydroxide solution to the sodium bisulfite solution already in the crystallizer. Before operation, the electrodes were standardized with buffers of pH 4.01 and 6.86, respectively. Subsequently, the solution was adjusted to a desired pH value by adding 0.1 M NaOH or 0.1 M HCl solution. All the chemicals were extra pure reagent grade from Kokusan Chemical Works. Nucleation was initiated by the introduction of a known amount of titrant into the supersaturated solution, and the crystallization process changed to crystal growth at the latter stage of operation. The pH was kept constant during operation using a pH-stat apparatus (Kyoto Electronic AT 200) to control the amount of calcium hydroxide solution added into the crystallizer. In order to prevent the oxidation of sulfite ion in the solution, sparging of nitrogen was continued during the precipitation operation. The operating variables were pH, solution concentration, and concentration of EDTA. To simulate the industrial scrubbing liquor composition (LaMantia et al., 1975), the concentration of total sulfite was kept in large excess. In addition, the operating pH range, from 5.80 to 6.80, was similar to that of the scrubbing solution. All the operating conditions were listed in Table 1.

Table 1. Operating Conditions and Crystal Properties in the Crystallization of Calcium Sulfite Hemihydrate Crystals

Operating Conditions	
total sulfite concentration at initial stage (TSO)	40–80 mM
total calcium concentration at initial stage (TCA)	2.80–3.75 mM
concentration of EDTA	0–2.45 mM
pH range	5.8–6.8
temperature	25 °C
agitation rate	400 rpm
operating time	120–130 min
Crystal Properties	
crystal habit	platelet
crystal system	orthorhombic
main peak strength	2.62, 3.16, 3.81, 5.35, 5.56 Å
crystal density	1390 kg/m^3
mass weight mean size	33.86–68.34 μm
BET specific surface area (SSA)	0.32–1.40 m^2/g

At the end of operation, the slurry was filtered and the solids were dried in an oven at 110 °C for at least 1 h. Particle morphology and solid composition were examined by SEM, IR spectroscopy, and X-ray powder diffraction. In addition, particle size distribution was analyzed by the Microtrac sizer. The calcium ion concentration was determined by EDTA potentiometric titration using a combined F-2002 calcium ion selective electrode and a K-401 reference electrode connected to a PHM 82 digital pH meter, all from the Radiometer Co. The specific surface area of the grown crystals was determined by the multiple-point BET technique (Micromeritics, 2100D). Besides, the titration curve obtained automatically at the latter stage of operation was employed to calculate the crystal growth rates.

Determination of Relative Supersaturation and Crystal Growth Rate

The relative supersaturation defined by Nielsen and Toft (1984) is given by

$$\sigma = (IP^{1/2} - K_{sp}{}^{1/2})/K_{sp}{}^{1/2} \quad (1)$$

Table 2. Equilibrium Equations and Stability Constants for the $Ca(OH)_2/NaHSO_3$ System at 25 °C (Lowell, 1970)

Mass Balance Equations

$$TCA = [Ca^{2+}] + [CaOH^+] + [CaSO_3^0] \quad (2)$$

$$TSO = [H_2SO_3] + [HSO_3^-] + [SO_3^{2-}] + [CaSO_3^0] \quad (3)$$

$$TNA = [Na^+] + [NaOH] \quad (4)$$

$$TCI = [Cl^-] \quad (5)$$

Mass Action Equations

$$pK_1 = -\log y_1^2 [H^+][OH^-] = 14.00 \quad (6)$$

$$pK_2 = -\log\left(\frac{y_1^2[H^+][HSO_3^-]}{y_0[H_2SO_3]}\right) = 1.88 \quad (7)$$

$$pK_3 = -\log\left(\frac{y_2[H^+][SO_3^{2-}]}{[HSO_3^-]}\right) = 7.21 \quad (8)$$

$$pK_4 = -\log\left(\frac{y_2^2[Ca^{2+}][SO_3^{2-}]}{y_0[CaSO_3^0]}\right) = 3.39 \quad (9)$$

$$pK_5 = -\log\left(\frac{y_2[Ca^{2+}][OH^-]}{[CaOH^+]}\right) = 1.37 \quad (10)$$

$$pK_6 = -\log\left(\frac{y_1^2[Na^+][OH^-]}{y_0[NaOH]}\right) = -0.57 \quad (11)$$

$$pK_{sp} = -\log(y_2^2[Ca^{2+}][SO_3^{2-}]) = 6.61 \quad (12)^a$$

[a] The value was calculated from the data that were reported by Brewer (1982) in *Flue Gas Desulfurization*.

where IP = $(Ca^{2+})(SO_3^{2-})$ and K_{sp} is the solubility product. Using mass action equations, which are presented in Table 2, and mass balance equations, the concentrations of all species in solution were computed from the measured pH, total calcium concentration, total sulfite concentration, and total sodium concentration by successively approximating the ionic strength (Nancollas, 1966). The ionic activity coefficients were estimated from the modified Debye–Hückel equation:

$$\log y_z = -AZ^2\left(\frac{\sqrt{I}}{1+\sqrt{I}}\right) - 0.3I \quad (13)$$

where y_z is the activity coefficient of the ion with charge z and A is a constant.

The growth rate of $CaSO_3$ can be expressed as the consumption rate of total sulfite concentration (TSO):

$$-\frac{J}{V} = \frac{d[TSO]}{dt} = \frac{d[CaSO_3^0]}{dt} + \frac{d[H_2SO_3]}{dt} + \frac{d[HSO_3^-]}{dt} + \frac{d[SO_3^{2-}]}{dt} \quad (14)$$

where J and V are molar growth rate and solution volume, respectively. Because the change of total sulfite concentration in the crystallizer is equal to the consumption of calcium concentration in the burette of the pH-stat apparatus and the total concentration of calcium ion in the crystallizer, the material balance on the total calcium ion is

$$-\frac{1}{V}\frac{dn_b}{dt} = \frac{d[Ca^{2+}]}{dt} + \frac{d[CaSO_3^0]}{dt} + \frac{d[CaOH^+]}{dt} - \frac{d[CaSO_3(s)]}{dt} \quad (15)$$

Because the growth rate $d[CaSO_3(s)]/dt$ is equal to the consumption rate of TSO, i.e. $d[TSO]/dt$, the molar growth rate can be derived (see Appendix)

$$J = f\frac{dn_b}{dt} = fC_b\frac{dV_b}{dt} \quad (16)$$

and the growth rate per unit crystal surface area is defined as

$$R_g = \frac{J}{A} = \frac{fC_b}{M_t V(SSA)}\frac{dV_b}{dt} \quad (17)$$

where f is a constant and is calculated from the concentration of ion species using eq A-19, C_b is the concentration of titrant, and dV_b/dt is the titration rate, which is the slope of the titration curve. In addition, M_t and SSA are magma density and the corresponding specific surface area of crystals, respectively.

Results and Discussion

Solid Composition of Platelet Crystals. Twenty-one runs were conducted in this work. The precipitate produced at given conditions was examined by IR spectroscopy and X-ray powder diffraction. In all runs, the IR spectra showed that the major band appeared at 990 cm^{-1} which is a standard peak (Vandeberg, 1983) for calcium sulfite hemihydrate. No trace of calcium sulfate was found in this work. The X-ray diffraction pattern has also demonstrated that calcium sulfite hemihydrate was the only crystal present in the system throughout the experiments. A typical spectrum of an X-ray pattern is shown in Figure 2. The main peaks as indicated are close to the standard values for calcium sulfite hemihydrate (McClune, 1983).

The SEM photographs show that the crystals are platelets and their agglomerates, which are presented in Figure 3, in all runs. The platelet form of calcium sulfite hemihydrate crystal was found in a supersaturated solution in which the total sulfite concentration ranges from 40 to 80 mM and the pH values were in the range of 5.8–6.8. The result is similar to that reported by Tseng and Rochelle (1986) where the morphology of calcium sulfite hemihydrate is a spherical agglomerate of thick platelet from a different reaction system, $CaCl_2/Na_2SO_3/H_2O$, in the absence of sulfate.

Titration Curves and Induction Period. Upon mixing of the calcium hydroxide solution with the sodium bisulfite solution, the precipitation process started within 20 min for most runs. As shown in Figure 4, which shows the titration curves, the induction time varied from run to run, about 8 min for runs 7 and 5 but no appreciable induction time for run 14. The difference was caused by the starting supersaturation, which is higher for run 14. Such a result has been suggested by Mullin (1972). The titration curves for all runs can be divided into two regions as indicated in Figure 4, a faster titration rate followed by a slower one. The steep slope of the titration curve in the first region indicated the occurrence of spontaneous nucleation,

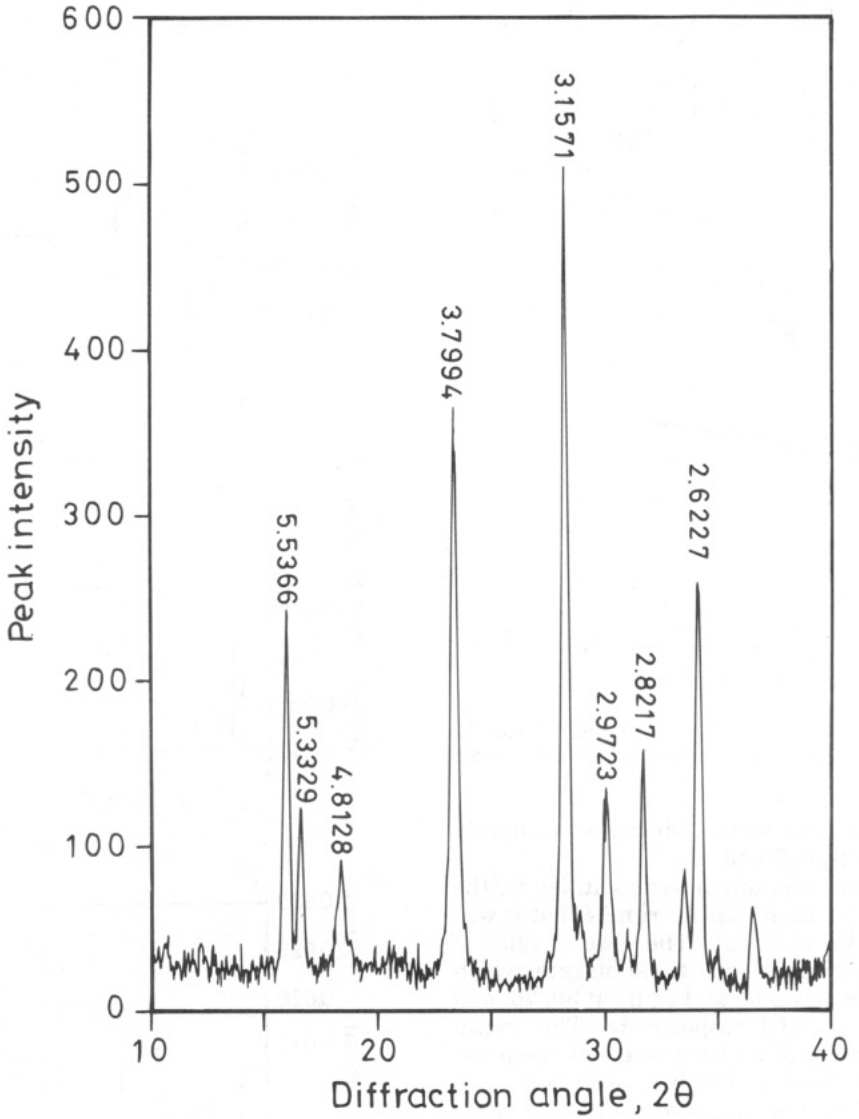

Figure 2. X-ray powder diffraction pattern of calcium sulfite hemihydrate crystals for run 2.

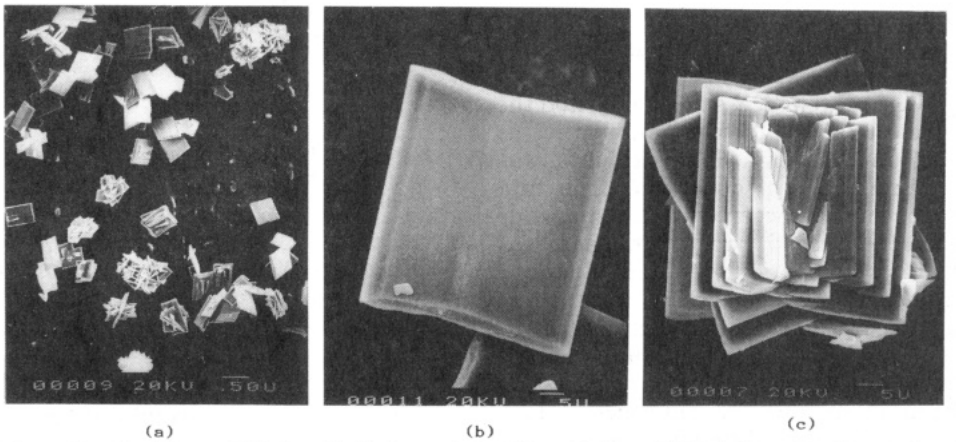

(a) (b) (c)

Figure 3. SEM photographs of calcium sulfite hemihydrate crystals: (a) a mixture of platelets and agglomerates, (b) platelet crystal, and (c) agglomerate crystal.

which was similar to that reported by Klepetsanis and Koutsoukos (1989) for the precipitation of calcium sulfate dihydrate and Frèche and Heughebaert (1989) for calcium phosphate precipitation. The spontaneous nucleation stopped until the relative supersaturation became a lower value where the crystal growth was prevailing. The primary nuclei produced in the crystallizer were utilized as the seed crystals for further crystal growth.

The amount of titration volume at the first region within 30 min for run 14 was higher than that for runs 5 and 7. The possible reason was that a large amount of nuclei was induced immediately for run 14 at a high supersaturation level ($\sigma_i = 1.36$) and the pH became lower due to the consumption of reactants. Therefore, a compensation of more basic solution (titrant, $Ca(OH)_2$ solution) by the autotitrator was required to keep the pH constant during the precipitation process. On the

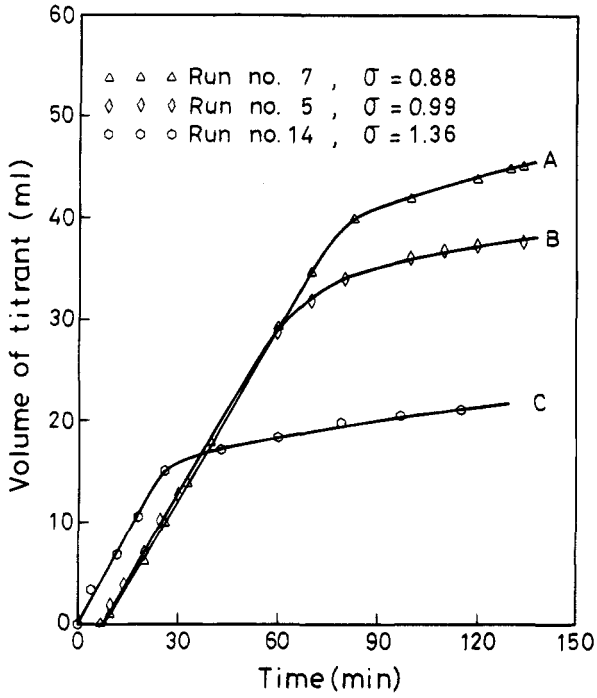

Figure 4. Titration curves of $Ca(OH)_2$ at different pH levels: curve A, pH = 6.20; curve B, pH = 6.50; and curve C, pH = 6.80.

other hand, fewer nuclei were induced at moderate supersaturation for runs 5 and 7.

As a result, the consumptions of basic solution for the two runs were smaller than that for run 14, but it was enough to keep the pH constant. The second region of the titration curves with a slower titration rate, which is probably due to crystal growth, begins at 30, 70, and 80 min for runs 14, 5, and 7, respectively. The crystal growth process occurred at an early stage of operation for run 14 because excess nuclei with large surface areas were induced to reduce the supersaturation to a lower level, which was unable to cause nucleation. The final supersaturation was 0.05, 0.34, and 0.46 for runs 14, 5, and 7, respectively.

Crystal Size Distribution and Degree of Agglomeration. The crystal size distribution data determined by the Microtrac particle size analyzer on the volume basis were converted to weight intensities as shown in Figures 5 and 6. A bimodal distribution was observed at the final stage of operation. The first population peak appeared between 0 and 20 μm, while the size range of the second population peak was between 20 and 100 μm. Under different pH values and EDTA concentrations, the change of CSD indicated the occurrence of agglomeration. Evidence in Figure 3c shows that the agglomerates are many small platelets growing out from a common center to form a spherelike particle and contain many internal void spaces. However, parts of the agglomerates show multiple platelets growing out from one platelet, but not enough to form a sphere.

The degree of agglomeration can be assessed either in terms of the number-based degree of agglomeration (Budz et al., 1987; Hartel et al., 1986) or in terms of the dominant size of the particles, i.e. the higher the particle size, the higher the agglomeration rate (Budz et al., 1987). The agglomerates of calcium sulfite comprising many platelet crystals were mostly growing out from a common center as shown in Figure 3c. The number of crystals involved in one agglomerate was

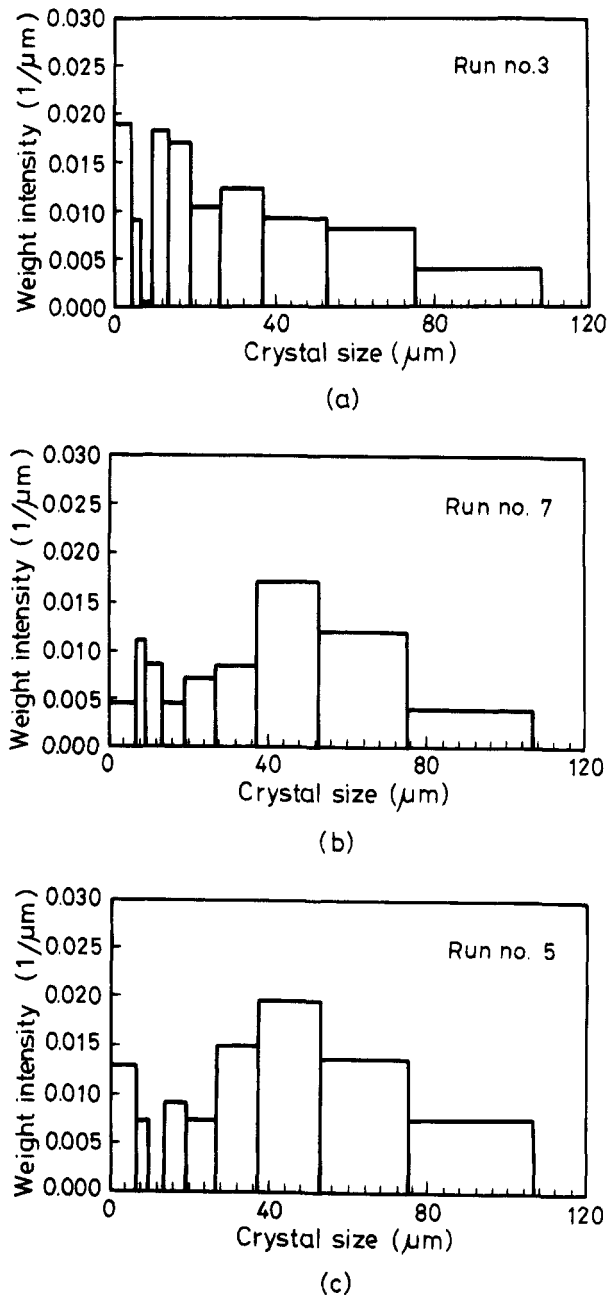

Figure 5. Effect of pH on the CSD at the same concentration level with TSO = 40 mM and TCA = 3.75 mM: (a) run 3 with pH = 5.80, (b) run 7 with pH = 6.20, and (c) run 5 with pH = 6.50.

difficult to estimate. Therefore, instead of the number-based degree of agglomeration, the mass-based degree of agglomeration was utilized, which is defined as

$$P = \frac{\text{weight of particles larger than } 16\ \mu\text{m}}{\text{weight of product}} \quad (18)$$

The particle size larger than 16 μm was considered as agglomerate because the weight intensity was the lowest around 16 μm in most of the cases in Figures 5 and 6. Meanwhile, the mean size, $L_{4,3}$, was also used to assess the degree of agglomeration as adopted by Budz et al. (1987) and Hartel et al. (1986). It was inferred that the degree of agglomeration was a function of magma density, M_t, initial relative supersaturation, σ_i, and pH value. From the data of CSDs, P and $L_{4,3}$ were calculated and are listed in Table 3. Values of $L_{4,3}$ and N referred to the agglomeration parameters in this

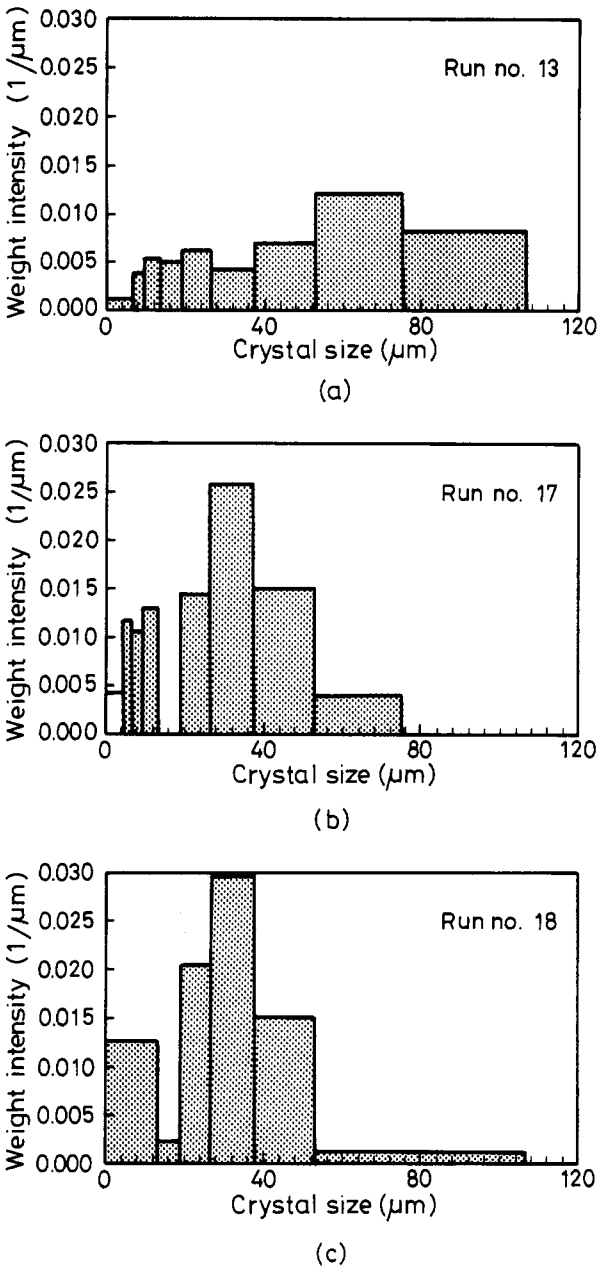

Figure 6. Influence of EDTA on the CSD at pH = 6.80 and the same concentration with TSO = 40 mM and TCA = 3.75 mM: (a) run 13 with EDTA = 0 mM, (b) run 17 with EDTA = 1.50 mM, (c) run 18 with EDTA = 2.45 mM.

work. When agglomeration occurs, a decrease in the total number of particles, N, and an increase in the number of large particles would be observed, while the mass-weighted average size, $L_{4,3}$, would be increased with an increase in the number of large particles. Thus, a smaller N or a larger $L_{4,3}$ indicates a strong agglomeration behavior in the crystallization process.

A multiple linear regression analysis from the agglomeration data gave the following correlations:

$$P = 0.6755\sigma_i^{0.0634} M_t^{0.0515} \exp[0.0548\ \mathrm{pH}] \quad (19)$$

and

$$L_{4,3} = 4.8496\sigma_i^{0.0695} M_t^{0.0453} \exp[0.3746\ \mathrm{pH}] \quad (20)$$

The measured values, P_{mea} and $(L_{4,3})_{mea}$, are compared with the calculated values, P_{cal} and $(L_{4,3})_{cal}$, as shown

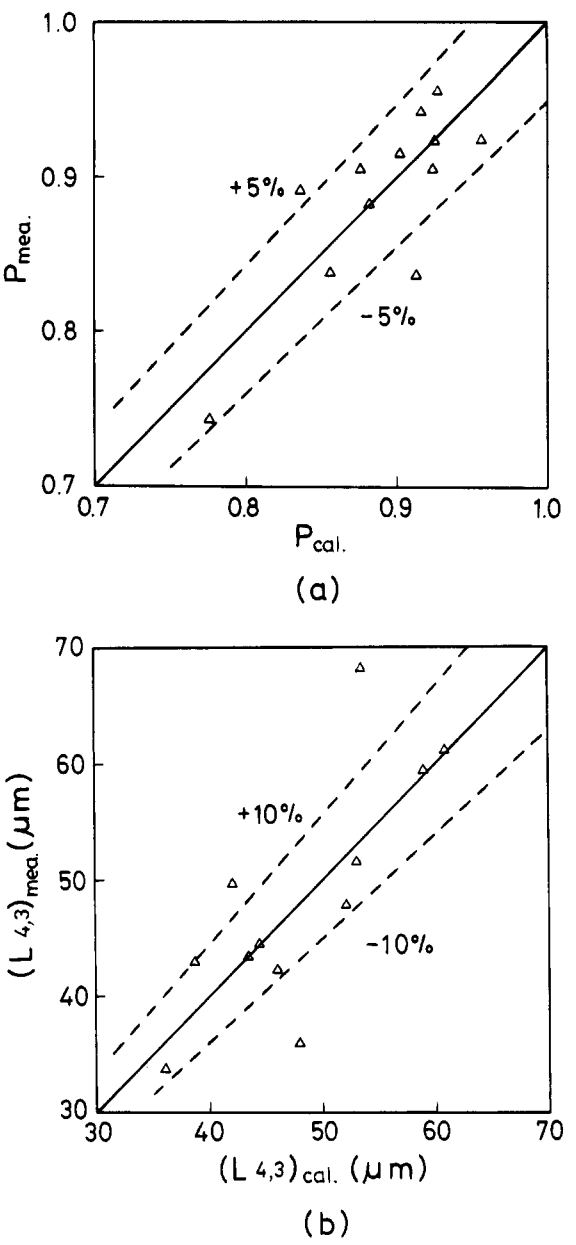

Figure 7. Calculated values vs measured values for P and $L_{4,3}$ (a) using eq 19 for P and (b) using eq 20 for $L_{4,3}$.

in Figure 7; most data points fall within ±10% of the calculated values. The low values of the parameters in these correlations show that the influence of supersaturation and magma density on the degree of agglomeration is not great. This can be explained as follows. In the ranges of operating conditions, the changes in $\sigma_i^{0.0634}$ and $M_t^{0.0453}$ are 1.05 for the former and 1.10 for the latter, while the changes in exp[0.0548 pH] and exp[0.3746 pH] are 1.06 and 1.45 for P and $L_{4,3}$, respectively. This indicated that the effects of σ_i and M_t on the degree of agglomeration are not significant. On the other hand, the pH value is the most sensitive factor affecting the degree of agglomeration during the precipitation. As shown in Figure 5, the CSD was a function of pH at the same solution concentration. It was found that the bimodal CSD was significant and disappeared gradually when the solution pH increased. In addition, the weight intensity of the large crystal size was also increased with increasing solution pH. This was caused by agglomeration. The dependence of agglomeration on pH is probably due to the change of

Table 3. Operating Variables, Growth Rates, and Agglomeration Parameters of Calcium Hemihydrate Crystals at Initial and Final Stages

		solution compositions (mM)							M_t	SSA	R_g (10^{10})		$L_{4,3}$[a]	N/M_t (10^{-4})[b]
run no.	pH	H_2SO_3 ($\times 10^3$)	HSO_3^-	Ca^{2+}	SO_3^{2-}	$CaSO_3^0$	Na^+	σ	(kg/m^3)	(m^2/g)	(mol/min/cm^2)	P	(μm)	(no./kg)
1	5.80	1.77	36.26	0.56	14.16	3.18	44.95	0.88	–		–	–	–	–
		1.71	35.32	0.16	13.67	0.87	43.85	0.50	0.15	0.46	14.25	0.89	43.12	26.91
2	6.50	1.78	36.24	0.57	14.22	3.18	46.87	1.32	–		–	–	–	–
		1.69	34.87	0.16	13.52	0.86	46.01	0.20	0.39	0.98	1.11	0.94	51.79	2.78
3	5.80	8.24	37.19	1.19	2.63	1.61	39.96	0.64	–		–	–	–	–
		7.87	35.77	1.20	2.51	1.58	38.98	0.62	0.05	1.40	18.18	0.74	33.86	81.30
4	6.80	1.02	37.20	0.26	32.21	2.53	47.10	1.06	–		–	–	–	–
		0.98	36.14	0.06	31.03	0.56	46.22	–	0.31	0.36	–	0.95	59.60	5.91
5	6.50	1.83	37.19	0.42	14.59	2.38	45.32	0.99	–		–	–	–	–
		1.70	35.19	0.19	13.61	1.07	43.70	0.34	0.27	0.44	2.92	0.91	47.98	43.47
6	6.00	5.26	37.19	0.90	4.22	1.89	39.94	0.77	–		–	–	–	–
		4.72	34.02	0.63	3.78	1.25	37.73	0.44	0.23	1.22	5.53	0.84	49.83	36.59
7	6.20	3.43	37.19	0.67	6.89	2.12	43.54	0.88	–		–	–	–	–
		3.15	34.78	0.38	6.34	1.16	41.66	0.46	0.25	0.56	5.54	0.91	42.40	25.37
8	6.20	3.31	36.24	0.91	6.65	2.84	39.97	1.17	–		–	–	–	–
		3.30	33.86	0.48	6.11	1.44	38.27	0.54	0.32	0.62	6.01	–	–	–
9	6.20	3.31	36.24	0.91	6.65	2.84	39.96	1.21	–		–	–	–	–
		3.07	34.28	0.40	6.19	1.23	38.57	0.43	0.34	0.40	6.82	–	–	–
10	6.50	1.78	36.25	0.57	14.22	3.18	47.01	1.30	–		–	–	–	–
		1.66	34.34	0.27	13.27	1.44	45.37	0.55	0.33	0.58	5.03	0.93	68.34	33.13
12	6.00	5.13	36.24	1.23	4.11	2.52	40.12	1.04	–		–	–	–	–
		4.64	33.47	0.65	0.72	1.27	37.98	0.44	0.29	0.42	7.64	0.88	43.53	53.68
13	6.50	1.75	36.24	0.56	14.03	3.19	39.94	1.30	–		–	–	–	–
		1.61	33.83	0.34	12.86	1.87	38.14	0.77	0.30	0.32	5.44	–	–	–
14	6.80	0.98	35.64	0.36	30.97	3.31	56.02	1.36	–		–	–	–	–
		0.93	34.43	0.07	2.96	0.65	53.63	0.05	0.43	0.41	1.80	0.93	61.30	20.62
15	6.20	3.32	36.24	0.91	6.68	2.83	41.99	1.17	–		–	–	–	–
		3.13	34.73	0.32	6.31	0.99	40.82	0.28	0.36	1.24	1.78	0.84	36.08	51.28
16	6.00	13.12	76.23	0.90	10.38	2.84	86.03	1.18	–		–	–	–	–
		12.83	75.59	0.34	10.19	1.07	81.74	0.34	0.38	1.20	2.54	0.92	44.66	26.20

[a] $L_{4,3} = \int_L^\infty L^4 n(L)\,dL / \int_L^\infty L^3 n(L)\,dL$ which was evaluated by the numerical integration. [b] $N = \int_L^\infty n(L)\,dL$ which was evaluated by the numerical integration.

electrical charge on the crystal surface. At higher pH, more HSO_3^- ions are shifted to SO_3^{2-}, thus giving a higher relative supersaturation and reducing the amount of HSO_3^- adsorbed on the crystal surface. The solutes higher in supersaturation would induce more nuclei which would give the ions more chances to collide with each other. Subsequently, the collision between crystals may begin to create agglomerates, thus yielding more large agglomerates, because the electrical charge is neutralized with a decrease in calcium ion. Further evidence about the degree of agglomeration is that the $L_{4,3}$, mass weight mean size, increased with decreasing N/M_t, particle numbers per unit product of solid, as shown in Figure 8. The small particle numbers with a large mean particle size, $L_{4,3}$, were due to the agglomeration of crystals (Hartel et al., 1986; Budz et al., 1987).

The addition of EDTA was found to be a factor that influenced the CSD. Figure 6 illustrates the effect of EDTA on the CSD at the same pH and initial solution concentration. A bimodal CSD was observed as the concentration of EDTA increased. On the other hand, the ratio N/M_t increased with increasing EDTA as indicated in Figure 9. This evidence shows that the degree of agglomeration is attenuated by the addition of EDTA. Theoretically, one EDTA molecule chelates one calcium ion to reduce the free calcium ion in the solution and thus to decrease the supersaturation. Another possible reason is that the adsorption of anionic ion (EDTA) on the positively charged surfaces of calcium sulfite crystals affects the electrical potential of the salt nuclei. Once the nuclei are brought into contact by collision, the adsorbed EDTA might reduce the agglomeration rate by altering the electrical double layer (Dirksen and Ring, 1991).

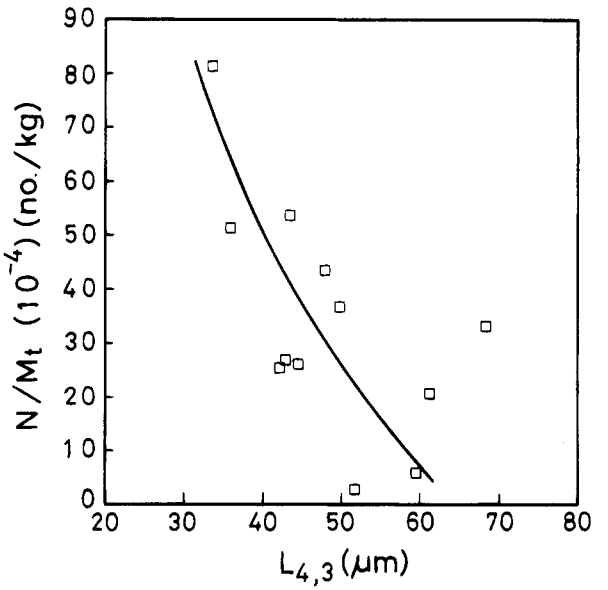

Figure 8. Plot of N/M_t vs $L_{4,3}$.

Growth Rate of Calcium Sulfite Hemihydrate. The growth rates of calcium sulfite hemihydrate crystals were calculated from the titration curves, by example, shown in Figure 4. The titration curves in Figure 4 are almost linear in the second region. The slopes obtained for curves A, B, and C in the second region are 0.075, 0.036, and 0.034 mL/min, respectively. These values together with the values of f and C_b can be utilized to calculate the molar growth rates using eq 16. Then, the molar growth rates of crystals per unit surface area of crystals, calculated by eq 17, are summarized in Table

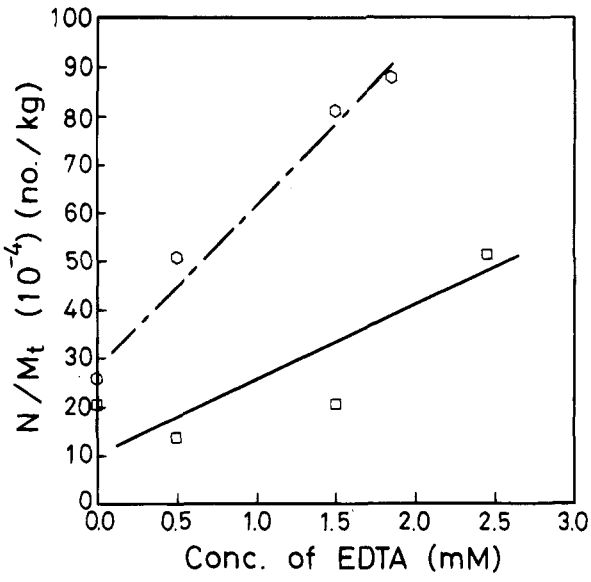

Figure 9. Effect of EDTA on the degree of agglomeration: ○, TSO = 80 mM and TCA = 3.75 mM; □, TSO = 40 mM and TCA = 3.75 mM.

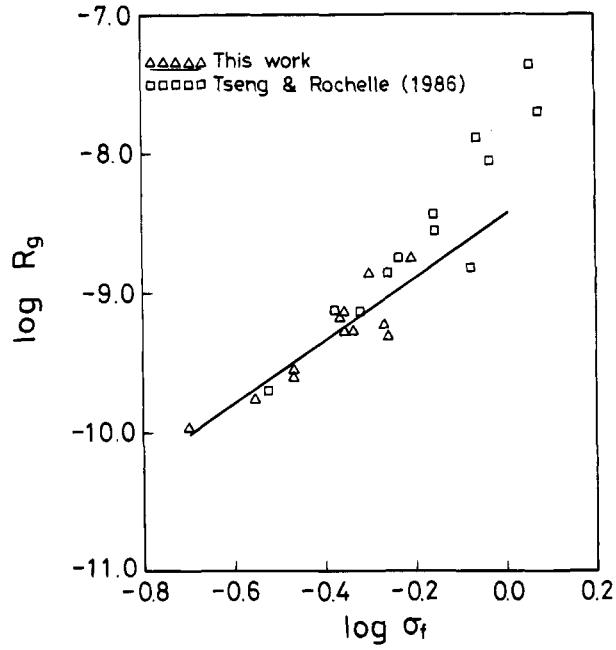

Figure 10. Overall growth rate of calcium sulfite hemihydrate crystals at 25 °C: △, this work; □, recalculated data from Figure 6 of Tseng and Rochelle (1986).

3. For sparingly soluble salts, the growth rate is usually expressed as follows:

$$R_g = k\sigma^n \tag{21}$$

Generally, the growth data of calcium sulfite hemihydrate crystals are plotted as ln R_s vs ln σ. In order to compare the data obtained from Tseng and Rochelle (1986), recalculation of supersaturation is required. The growth rate data of both works were plotted in Figure 10. In the supersaturation range under investigation, σ between 0.05 and 0.77, the linear plot gave $n = 2.26$ and $k = 3.68 \times 10^{-9}$ mol/min cm^2. The data are quite close to the values reported by Tseng and Rochelle (1986) in the low supersaturation range, where it obeys a parabolic rate law. The growth mechanism of $CaSO_3 \cdot {}^1/_2H_2O$ at low supersaturation obeyed the parabolic rate law, which is the same as that of many sparingly soluble substances, including calcium carbonate, gypsum, calcium fluorite, and barium sulfate (Nielsen, 1984). A different result was reported by Ottmers (1974) and Phillips (1978) who found that the linear rate law was observed for the crystal growth of $CaSO_3 \cdot {}^1/_2H_2O$. The BCF theory states that the linear rate law occurs at higher relative supersaturation, while the parabolic rate law occurs in most cases of lower relative supersaturation. The different rate laws obtained in this work and others may be due to different techniques and reactants utilized in the experiments to determine the growth rate data.

Conclusion

The semibatch precipitation of calcium sulfite hemihydrate from aqueous solution is successfully conducted in a pH-stat apparatus to study the degree of agglomeration and crystal growth of calcium sulfite hemihydrate. The precipitates were platelets and their agglomerates in all runs under the operating conditions listed in Table 1. The crystal growth kinetics was found to obey the parabolic rate law, in agreement with BCF theory at lower relative supersaturation. The effect of relative supersaturation and magma density on the degree of agglomeration is not significant at the final stage of operation, while the pH factor has a significant effect. Besides, the addition of EDTA is also a factor that affects the degree of agglomeration.

Nomenclature

A = area, m^2
C_b = concentration of $Ca(OH)_2$ added from burette, kmol/m^3
f = constant in eq 16
f_i = constant defined in Appendix A
I = ionic strength, kmol/m^3
IP = ionic product
J = molar growth rate, mol/min
k = growth rate constant, mol/min cm^2
K_i = stability constant in Table 2
K_{sp} = solubility product
$L_{4,3}$ = mass weight mean size, μm
M_t = magma density, kg/m^3
n = population density, no./μm m^3
n_b = molar number of $Ca(OH)_2$ added from burette, mol
N = total particle numbers, no./m^3
R_g = growth rate per unit area, mol/min cm^2
SSA = specific surface area, m^2/g
TCA = total calcium ion concentration, kmol/m^3
TCI = total chloride ion concentration, kmol/m^3
TNA = total sodium ion concentration, kmol/m^3
TSO = total sulfite ion concentration, kmol/m^3
t = time, min
V = volume of solution, m^3
V_b = volume of $Ca(OH)_2$ added from burette, mL
y_z = activity coefficient of an ion with charge z
Z = charge number

Appendix A

Derivation of Eq 17 for Estimating Crystal Growth Rate. From eqs 7−9 in Table 2, the following

relationships are obtained:

$$[H_2SO_3] = \frac{y_1^2[H^+][HSO_3^-]}{K_2 y_0} \quad \text{(A-1)}$$

$$[SO_3^{2-}] = \frac{K_3[HSO_3^-]}{y_2[H^+]} \quad \text{(A-2)}$$

$$[CaSO_3^0] = \frac{y_2^2[Ca^{2+}][SO_3^{2-}]}{K_4 y_0} \quad \text{(A-3)}$$

We substitute the above equations into eq 3 to give

$$-\frac{J}{V} = f_1\frac{d[HSO_3^-]}{dt} + f_2\frac{d[Ca^{2+}]}{dt} \quad \text{(A-4)}$$

where

$$f_1 = 1 + \frac{K_3}{y_2[H^+]} + \frac{y_2^2[H^+]}{K_2 y_0} + \frac{K_3 y_2[Ca^{2+}]}{K_2 y_0[H^+]} \quad \text{(A-5)}$$

and

$$f_2 = \frac{y_2^2[SO_3^{2-}]}{K_2 y_0} \quad \text{(A-6)}$$

The growth rate of calcium sulfite hemihydrate is equal to the consumption of TSO:

$$\frac{d[CaSO_3(s)]}{dt} = -\frac{d[TSO]}{dt} = \frac{d[CaSO_3^0]}{dt} + \frac{d[H_2SO_3]}{dt} + \frac{d[HSO_3^-]}{dt} + \frac{d[SO_3^{2-}]}{dt} \quad \text{(A-7)}$$

Equation A-7 is substituted into eq 15 to give

$$-\frac{1}{V}\frac{dn_b}{dt} = \frac{d[Ca^{2+}]}{dt} + \frac{d[CaSO_3^0]}{dt} + \frac{d[CaOH^+]}{dt} - \frac{d[CaSO_3(s)]}{dt}$$

$$= \frac{d[Ca^{2+}]}{dt} + 2\frac{d[CaSO_3^0]}{dt} + \frac{d[CaOH^+]}{dt} + \frac{d[SO_3^{2-}]}{dt} + \frac{d[H_2SO_3]}{dt} + \frac{d[HSO_3^-]}{dt} \quad \text{(A-8)}$$

From eq 10, we have

$$[CaOH^+] = \frac{y_2[Ca^{2+}][OH^-]}{K_5} \quad \text{(A-9)}$$

Then, $[CaSO_3^0]$, $[SO_3^{2-}]$, $[H_2SO_3]$, and $[CaOH^+]$ in eq A-8 were eliminated by using eqs A-1−A-3 and A-9. The resultant equation is

$$-\frac{1}{V}\frac{dn_b}{dt} = f_3\frac{d[HSO_3^-]}{dt} + f_4\frac{d[Ca^{2+}]}{dt} \quad \text{(A-10)}$$

where

$$f_3 = \left(1 + \frac{y_1^2[H^+]}{K_2 y_0}\right) + \frac{K_3}{y_2[H^+]}\left(1 + \frac{2[Ca^{2+}]y_2^2}{K_4 y_0}\right) \quad \text{(A-11)}$$

and

$$f_4 = 1 + \frac{2y_2^2[SO_3^{2-}]}{K_4 y_0} + \frac{y_2[OH^-]}{K_5} \quad \text{(A-12)}$$

The electroneutrality of nonreacting components in the crystallizer is

$$2\frac{d[SO_3^{2-}]}{dt} + \frac{d[HSO_3^-]}{dt} = 2\frac{d[Ca^{2+}]}{dt} + \frac{d[CaOH^+]}{dt} \quad \text{(A-13)}$$

When eqs A-2 and A-9 are substituted into eq A-13, the following relationship is obtained:

$$\frac{d[HSO_3^-]}{dt} = f_5\frac{d[Ca^{2+}]}{dt} \quad \text{(A-14)}$$

where

$$f_5 = \frac{2 + y_2[OH^-]/K_5}{1 + 2K_3/y_2[H^+]} \quad \text{(A-15)}$$

Substituting eq A-14 into eqs A-4 and A-10 to eliminate $d[HSO_3^-]/dt$, we obtain the following equations:

$$-\frac{J}{V} = (f_1 f_5 + f_2)\frac{d[Ca^{2+}]}{dt} \quad \text{(A-16)}$$

and

$$-\frac{1}{V}\frac{dn_b}{dt} = (f_3 f_5 + f_4)\frac{d[Ca^{2+}]}{dt} \quad \text{(A-17)}$$

Compare eqs A-16 and A-17 to give

$$J = f\frac{dn_b}{dt} \quad \text{(A-18)}$$

where

$$f = \frac{f_1 f_5 + f_2}{f_3 f_5 + f_4} \quad \text{(A-19)}$$

The molar growth rate per unit area is

$$R_g = \frac{J}{A} = \frac{f}{A}\frac{dn_b}{dt} \quad \text{(A-20)}$$

Appendix B

Calculation of K_{sp} of $CaSO_3 \cdot {}^1/_2H_2O$ at 298 K. The solubility product of calcium sulfite hemihydrate crystals was obtained from thermal data reported by Brewer. The reaction equation is

$$CaSO_3 \cdot {}^1/_2H_2O(s) \rightarrow Ca^{2+} + SO_3^{2-} + {}^1/_2H_2O(1) \quad \text{(B-1)}$$

The solubility product was evaluated by the following equation:

$$\ln K_{sp} = -\Delta G^\circ/RT = -\Delta(G^\circ - H^\circ_{298}/RT) - (\Delta H^\circ_{298}/RT) \quad \text{(B-2)}$$

Table B-1. Thermal Data Adopted from Brewer[a]

components	$-(G^\circ - H^\circ_{298})/RT$	$-(G^\circ - H^\circ_{298})/RT$ (T = 298 K or 25 °C)	$(\Delta H^\circ_{298}/RT)$
$CaSO_3{\cdot}^1/_2H_2O$	$22.5 - 6.24 \times 10^{-2}T + 1.53 \times 10^{-4}T^2 - 1.07 \times 10^{-7}T^3$ (T in K)	14.66	−528.18
Ca^{2+}	$-6.75 + 1.0 \times 10^{-3}t - 2.2 \times 10^{-5}t^2 + 2 \times 10^{-8}t^3$ (t in °C)	−6.24	−219.03
SO_3^{2-}	$-4.4 + 1.18 \times 10^{-2}t - 1.98 \times 10^{-4}t^2 + 3.2 \times 10^{-7}t^3$ (t in °C)	−4.22	−257.18
H_2O	$18.025 - 8.867 \times 10^{-2}T + 2.8856 \times 10^{-4}T^2 - 3.9505 \times 10^{-7}T^3 + 2.08 \times 10^{-10}T^4$ (T in K)	8.41	−115.36

[a] In *Flue Gas Desulfurization*, Chapter 1, ACS Symposium Series 188, edited by Hundson and Rochelle (1982).

where data $(G^\circ - H^\circ_{298})/RT$ and $(\Delta H^\circ_{298}/R)$ were the values reported by Brewer as shown in Table B-1. Therefore, values of $-\Delta(G^\circ - H^\circ_{298})/RT$ and $-(\Delta H^\circ_{298}/RT)$ were estimated as follows:

$$-\Delta[(G^\circ - H^\circ_{298})/RT] = -6.24 - 4.22 + {}^1/_2(8.41) - 14.66$$
$$= -20.92$$

and

$$-(\Delta H^\circ_{298}/RT) = -219.03 - 257.18 - {}^1/_2(115.36) + 528.18$$
$$= -5.71$$

Substituting the two values into eq B-2, the K_{sp} was obtained:

$$K_{sp} = 2.47 \times 10^{-7} \text{ at } 298 \text{ K}$$

Literature Cited

Beckman, J. R.; Farmer, R. W. Bimodal CSD Barite Due to Agglomeration in an MSMPR Crystallizer. *AIChE Symp. Ser.* **1987**, *83* (253), 85–94.

Brewer, L. Thermodynamic Values for Desulfurization Processes. *Flue Gas Desulfurization*; Hudson, J. L., Rochelle, G. T., Eds.; ACS Symposium Series 188; American Chemical Society: Washington, DC, 1982; pp 1–30.

Budz, J.; Jones, A. G.; Mullin, J. W. Effect of Selected Impurities on the Continuous Precipitation of Calcium Sulfate (Gypsum). *J. Chem. Technol. Biotechnol.* **1986**, *36*, 153–161.

Budz, J.; Jones, A. G.; Mullin, J. W. Agglomeration of Potassium Sulfate Crystals in an MSMPR Crystallizer. *AIChE Symp. Ser.* **1987**, *83* (253), 78–84.

Chen, P. C.; Tai, C. Y.; Shih, S. M. Control of Crystal Habit and Particle Morphology of Calcium Sulfite Hemihydrate Crystals. *J. Cryst. Growth* **1992**, *123*, 277–286.

Christoffersen, J.; Christoffersen, M. R. Kinetics of Spiral Growth of Calcite Crystals and Determination of the Absolute Rate Constant. *J. Cryst. Growth* **1990**, *100*, 203–211.

Dirksen, J. A.; Ring, T. A. Fundamentals of Crystallization: Kinetic Effects on Particle Size Distributions and Morphology. *Chem. Eng. Sci.* **1991**, *46*, 2389–2427.

Frèche, M.; Heughebaert, J. C. Calcium Phosphate Precipitation in The 60–80 °C Range. *J. Cryst. Growth* **1989**, *94*, 947–954.

Hartel, R. W.; Gottung, B. E.; Randolph, A. D.; Drach, G. W. Mechanisms and Kinetic Modeling of Calcium Oxilate Crystal Aggregation in a Urinelike Liquor. *AIChE J.* **1986**, *32*, 1176–1185.

Hostomsky, J.; Jones, A. G. Calcium Carbonate Crystallization, Agglomeration and Form During Continuous Precipitation from Solution. *J. Phys. D: Appl. Phys.* **1991**, *24*, 165–170.

Kazmlerczak, T. F.; Tomson, M. B.; Nancollas, G. H. Crystal Growth of Calcium Carbonate. A Controlled Composition Kinetic Study. *J. Phys. Chem.* **1982**, *86*, 103–107.

Klepetsanis, P. G.; Koutsoukos, P. G. Precipitation of Calcium Sulfate Dihydrate at Constant Calcium Activity. *J. Cryst. Growth* **1989**, *98*, 480–486.

Kralj, D.; Brecevic, L.; Nielsen, A. E. Vaterite Growth and Dissolution in Aqueous Solution. I. Kinetic of Crystal Growth. *J. Cryst. Growth* **1990**, *104*, 793–800.

LaMantia, C. R.; Lunt, R. R.; Shah, I. S. Dual Alkali Process for SO_2 Control. *AIChE Symp. Ser.* **1975**, *71* (148), 324–330.

McClune, W. F. *Powder Diffraction File Search Manual*; Hanawalt Method Inorganic: International Centre for Diffraction Data, 1983.

Mullin, J. W. *Crystallization*; Butterworth & Co.: London, 1972; Chapter 6.

Nancollas, G. H. *Interactions in Electrolyte Solution*; Elsevier: Amsterdam, 1966; Chapter 2.

Nielsen, A. E. Electrolyte Crystal Growth Mechanisms. *J. Cryst. Growth* **1984**, *67*, 289–310.

Nielsen, A. E.; Toft, J. M. Electrolyte Crystal Growth Kinetics. *J. Cryst. Growth* **1984**, *67*, 278–288.

Ottmers, D. A Theoretical and Experimental Study of the Lime/Limestone Wet Scrubbing Process. EPA Report 650/2-75-006; U.S. Government Printing Office: Washington, DC, 1974.

Phillips, J. L. Development of a Mathematical Basis for Relating Sludge Properties to FGD-Scrubber Operating Variables. EPA Report 600/7-78-072; U.S. Government Printing Office: Washington, DC, 1978.

Satriana, M. *New Developments in Flue Gas Desulfurization Technology*; Noyes Data Corp.: Park Ridge, NJ, 1981.

Söhnel, O.; Mullin, J. W. Agglomeration in Batch Precipitated Suspensions. *AIChE Symp. Ser.* **1992**, *87* (284), 182–190.

Tai, C. Y.; Chen, P. C. Nucleation, Agglomeration and Crystal Morphology of Calcium Carbonate. *AIChE J.* **1995**, *41*, 68–77.

Tai, C. Y.; Chen, P. C.; Shih, S. M. Size-Dependent Growth and Contact Nucleation of Calcite Crystals. *AIChE J.* **1993**, *39*, 1472–1482.

Tavare, N. S.; Garside, J. Silica Precipitation in a Semi-batch Crystallizer. *Chem. Eng. Sci.* **1993**, *48*, 475–488.

Tseng, P. C.; Rochelle, G. T. Calcium Sulfite Hemihydrate: Crystal Growth Rate and Crystal Habit. *Environ. Prog.* **1986**, *5*, 5–11.

Valencia, J. A. The Limestone Dual Alkali Process for Flue Gas Desulfurization. *ACS Symp. Ser.* **1982**, *188*, 325–347.

Vandeberg, J. T. *An Infrared Spectroscopy ATLAS for the Coatings Industry*; Federation of Societies for Coatings Technology: Philadelphia, PA, 1983.

Received for review March 28, 1994
Revised manuscript received December 30, 1994
Accepted January 13, 1995[⊗]

IE940207Z

[⊗] Abstract published in *Advance ACS Abstracts*, March 15, 1995.